

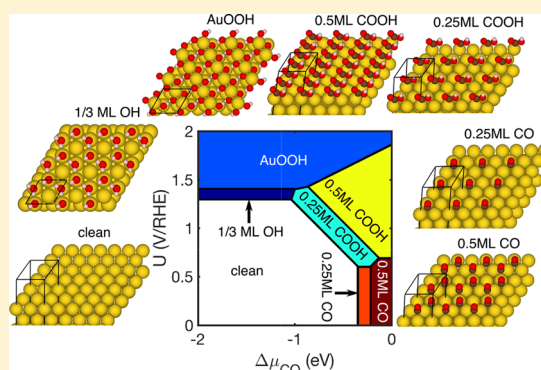
Calculations of the pH-Dependent Onset Potential for CO Electrooxidation on Au(111)

Zhiyao Duan and Graeme Henkelman*[✉]

Department of Chemistry and the Institute for Computational Engineering and Sciences, The University of Texas at Austin, Austin, Texas 78712-0165, United States

S Supporting Information

ABSTRACT: CO electrooxidation on the Au(111) surface exhibits an onset potential that depends strongly on the pH of the electrolyte. In alkaline solution, the onset potential for CO electrooxidation is found, experimentally, to be 0.5 V lower than in acidic media on the reversible hydrogen electrode scale. This phenomenon is explained here with density functional theory which is used to calculate adsorbate binding energies including the electric double layer of the Au(111)/aqueous interface. Our model consists of a charged Au(111) slab and implicit solvation for the electrolyte. The double reference method is used to determine the potential-dependent CO electrooxidation reaction energetics. A microkinetic model, based upon the calculated reaction energetics, confirms the lower onset potential in alkaline media. Our results show that there are three factors contributing to the lower onset potential in base: (1) stronger CO adsorption, (2) attraction between adsorbed CO and OH⁻, and (3) the high concentration of OH⁻ in base.



INTRODUCTION

pH-dependent activity and selectivity are commonly observed for many electrocatalytic reactions used in renewable energy conversion and storage applications. For example, hydrogen oxidation/evolution activity is found to decrease with pH.¹ The selectivity of CO₂ electrochemical reduction also strongly depends on the pH of the electrolyte.^{2–4} Motivated both by scientific curiosity regarding the origin of the pH-dependent properties and also a desire to improve rational catalyst design, there has been a large number of recent theoretical investigations on the pH-dependent activity and selectivity of electrocatalytic reactions.^{5–8} Here, we study CO electrooxidation on the Au(111) surface as a prototypical electrocatalytic reaction which exhibits strong pH-dependent activity.

Gold is an efficient catalyst for electrooxidation of CO dissolved in solution. Interestingly, CO electrooxidation on Au exhibits several unique characteristics. First, adsorbed CO on the Au surface enhances the adsorption of the oxidant (OH) and thus promotes its own oxidation.^{9,10} Second, electrooxidation of CO on Au exhibits strong pH-dependent onset potentials; i.e., in alkaline solution the onset potential for CO electrooxidation was found to be ca. 0.5 V versus the reversible hydrogen electrode (RHE), lower than that in acidic media.¹¹ The CO-enhanced OH binding on gold surfaces is demonstrated by additional peaks at 0.4 V/RHE in the voltammograms of CO-modified Au surfaces; these peaks are absent on bare Au surfaces.^{12,13} Theoretically, this effect is understood in terms of Au-mediated charge transfer from adsorbed CO to adsorbed OH.⁹ The pH dependence of the

onset potential was previously explained by stronger CO chemisorption under alkaline conditions where irreversible CO adsorption was observed. In turn, the adsorbed CO promotes the adsorption of OH and thus CO electrooxidation at lower applied potentials.¹⁴ In contrast, in acidic solutions, CO does not remain chemisorbed on the Au surface in the absence of CO in solution. Hence, OH adsorption occurs at higher potentials in acidic solutions. The stronger chemisorption of CO on Au was attributed to the different strength of the electric field in the electrical double layer (EDL) in acidic vs alkaline solutions.¹⁴ Indeed, at the same applied potential on the RHE scale, the true electric potential on the standard hydrogen electrode (SHE) scale is different in acidic and base solutions according to the relation

$$U_{\text{RHE}} = U_{\text{SHE}} + k_{\text{B}}T \ln(10)\text{pH}/e \quad (1)$$

For example, for $U_{\text{RHE}} = 1.0$ V at pH = 0 and pH = 14, the U_{SHE} are 1.0 and 0.17 V at standard conditions, respectively. The significant difference of U_{SHE} then leads to different strengths of the electric field in the EDL in acid and base solutions, assuming the width of the EDL remains constant. Density functional theory (DFT) calculations were performed to study the binding energy change of CO on Au surfaces in the presence of uniform electric fields.^{10,14} However, these calculations cannot provide a consistent explanation of all

Received: October 30, 2018

Revised: November 15, 2018

Published: November 21, 2018

experimental observations. Specifically, the binding energy of CO decreases by only -0.15 eV as the electric field decreases from 0 to -1.0 V/Å (a 3 V decrease of applied potential assuming an EDL width of 3 Å), which is insufficient to account for the observed irreversible CO adsorption on gold surface in base solution. Note that the assumption of a constant double layer width is only employed for this rough estimation of the voltage change; in reality, the double layer width varies with the applied potential. It should be noted that the binding energy of CO calculated under the assumption of a constant electric field is not a good description for the electrochemical system, which is typically held at a constant potential. CO adsorbates can significantly modify the Au work function, which results in different surface charges at the same potential. The difference in surface charge on CO-adsorbed surface versus bare Au surface is an important contribution to the binding energy of CO.

In this study, we performed DFT calculations, considering both potential and solvation effects, to study the pH-dependent onset potential of CO electrooxidation on the Au(111) surface. On the basis of the calculated reaction energetics and microkinetic modeling, we show an onset potential shift that is consistent with what is observed in experiments. From our calculations, we show that CO-induced OH adsorption, a stronger CO chemisorption in the alkaline solution, and a high concentration of OH⁻ together lead to the downshifting of the onset potential.

■ COMPUTATIONAL METHODS

Spin-polarized DFT calculations with a plane-wave basis set were performed using the Vienna *Ab initio* Simulation Package.^{15–17} The generalized gradient approximation functional of the Perdew–Wang 91¹⁸ form was used to describe the electronic exchange and correlation energy. Electron–ion interactions were treated with ultrasoft pseudopotentials.¹⁹ In all calculations, the energy cutoff of the plane wave basis set was 400 eV. The Brillouin zone was sampled using the Monkhorst–Pack scheme²⁰ with a $4 \times 4 \times 1$ k -point mesh for the $p(2 \times 2)$ Au(111) surface slab. We also employed a $(\sqrt{3} \times \sqrt{3})$ Au(111) surface slab, with the Brillouin zone sampled by a $6 \times 6 \times 1$ k -point mesh. Optimized structures were obtained by minimizing the forces on each ion until they fell below 0.01 eV/Å.

Structures of clean and adsorbate-covered Au(111) surfaces were simulated within the supercell approach using slabs consisting of five layers. The positions of the atoms in the middle layer were fixed during structure relaxation. Adsorbates were introduced on both the top and the bottom layer to construct a symmetric slab to eliminate the electric dipole between the periodic surface layers. A 20 Å vacuum layer was used to separate periodic images of the slabs. The lattice constant of Au was calculated to be 4.183 Å.

We employ the double-reference method to model the influence of the applied potential on the reaction energetics at the metal/solution interface.^{21,22} Different from the original implementation of the double-reference method, where explicit water molecules are used to model the metal/aqueous interface, the aqueous environment in this study is treated by the continuum solvation model developed by the Hennig group as implemented in the VASPsol code.²³ The linearized Poisson–Boltzmann background charge model has been recently implemented in VASPsol,²⁴ which better accounts

for the electronic shielding effect of electrolyte ions.²⁵ An essentially identical method has been employed to study the potential-dependent adsorption of CO₂ on Ni(111).²⁶ We set the relative permittivity of the solvent $\epsilon_{\text{solvent}}$ to 80 to account for the presence of the aqueous electrolyte. While this value corresponds to the permittivity of bulk water, we note that water at the metal/aqueous interface and the existence of electrolyte ions can cause the relative permittivity to deviate from the bulk value. A more accurate relative permittivity of the electrolyte can be simulated with both explicit water molecules and ions in solution. Unfortunately, the *ab initio* molecular dynamics simulations required to effectively sample the structures of the interfacial electrolyte are not computationally affordable at this time. Details of the double-reference method are provided in refs 21 and 22. Briefly, the electric potential of the simulated metal electrode is varied with the number of electrons in the system. To maintain charge neutrality of the supercell, a uniform background of compensating counter charge is added. The charged slab together with the compensating background charge polarizes the electrolyte near the metal/solution interface, creating an electrostatic potential profile that simulates the EDL. The electric potential of the slab referenced to the SHE is calculated as

$$U_q \text{ (V/SHE)} = -4.6 - \phi_q(f)/eV \quad (2)$$

where $-\phi_q(f)$ is the work function of the charged slab and 4.6 V is the work function of the H₂/H⁺ couple under standard conditions. Actually, measurements of the work function of the SHE are scattered from 4.4 to 4.8 V.²⁷ We select the average value of 4.6 V for our calculations, which also gives us a PZC for Au(111) consistent with experimental measurements, as shown in the Results section. To calculate $\phi_q(f)$, the as-calculated Fermi energy of the charged system $\phi_q^f(f)$ needs to be referenced twice to be properly referenced to the vacuum level. The first reference is the electrostatic potential in the middle of the solution phase far from the electrode. The absolute electrostatic potential in the middle of the solution is considered constant as a function of charge. The second reference point is the vacuum level in the uncharged calculation. The total energy of the charged system is then corrected for the interaction with the background charge as well as for the difference in the number of electrons in the system by

$$E_{\text{correction}} = \int_0^q \langle \overline{V}_{\text{tot}} \rangle dQ + qU_q \quad (3)$$

An additional energy correction for thick metal slabs has been proposed.²⁸ We examined the influence of this correction on the CO binding energies on the atop site of the Au(111) slab as shown in Figures S1 and S2 of the Supporting Information. We can see that the inclusion of the thick slab correction leads to a difference of <0.1 eV in the magnitude of the CO binding energy in the -1 to 1 V potential window. Because of the small effect of the thick slab correction, we did not include it in this study. We also tested the influence of a thicker Au slab (7 layers) on the CO binding energy as shown in Figure S3. The result shows that the binding energy difference is within 0.1 eV in magnitude in the -1 to 1 V potential window, which is again negligible in the context of this study.

For each structure, calculations are performed at charges of $-1|e|$ to $+1|e|$ at a step of $+0.2|e|$. The total free energy determined at each of the 11 points is then fit to a quadratic

equation to provide a continuous free energy as a function of potential. The quadratic form is consistent with a capacitor created by the charged-slab/background-charge system, which takes the form

$$E(U) = -\frac{1}{2}C(U - U_0)^2 + E_0 \quad (4)$$

where U_0 refers to the potential of zero charge (PZC), E_0 is the energy at the PZC, and C is the capacitance of the interface. From the fitted quadratic equations for the bare slab and adsorption models, the binding energies and reaction energetics as a function of electric potential are readily calculated.

With calculated binding energies, we also construct the surface phase diagram to understand the surface states of Au(111) under the reaction conditions of CO electrooxidation. This method is based upon the computational hydrogen electrode method^{29,30} and *ab initio* thermodynamics.³¹ Stable surface phases under reaction conditions are found by calculating their specific free energy of formation based on various proposed atomic structures of surface phases. The surface phases with the lowest free energies of formation as a function of adsorbate chemical potential and electrode potential will be present on the surface phase diagram. The specific free energy of formation is calculated as

$$\Delta\gamma = \frac{1}{A_S}(G_{\text{ads/slab}} - G_{\text{slab}} - \sum_i n_i \mu_i) \quad (5)$$

In eq 5, $G_{\text{ads/slab}}$ and G_{slab} are the Gibbs free energies of the adsorbate-covered and the clean surface, n_i is the number of adsorbed atoms of the type i per surface area A_S , and μ is the chemical potential of the adsorbates in their corresponding reservoir. In this study, we are concerned with the chemical potentials of CO, water, and oxygenated species generated through electrochemical water oxidation. The chemical potential of CO is determined from thermodynamic equilibrium with a gas-phase reservoir. Thus, the CO chemical potential depends on temperature and pressure according to

$$\mu_{\text{CO}}(T, p_{\text{CO}}) = E_{\text{CO}}^{\text{tot}} + \tilde{\mu}_{\text{CO}}(T, p^0) + k_B T \ln \frac{p_{\text{CO}}}{p^0} \quad (6)$$

where p^0 is the standard pressure, and $\tilde{\mu}_{\text{CO}}(T, p^0)$ is the chemical potential at p^0 , which is obtained from thermodynamical tables.³² The temperature- and pressure-dependent terms in eq 6 are further combined into one term, so that the chemical potential of CO is $\mu_{\text{CO}} = E_{\text{CO}}^{\text{tot}} + \Delta\mu_{\text{CO}}(T, p_{\text{CO}})$. The chemical potential of water in liquid phase at standard conditions is calculated as the chemical potential of a gas-phase water molecule at 0.035 bar because at this pressure, a gas-phase water molecule is in equilibrium with liquid water.²⁹ Hence, $\mu_{\text{H}_2\text{O}} = E_{\text{H}_2\text{O}}^{\text{tot}} + \Delta\mu_{\text{H}_2\text{O}}(T, 0.035 \text{ bar})$. The chemical potentials or electrochemical potentials of O and OH are calculated according to the electrochemical reactions



The electrochemical potential of the solvated proton and electron pair ($\text{H}^+ + \text{e}^-$) is calculated as $1/2\mu_{\text{H}_2} + eU_{\text{SHE}} - k_B T \ln(10)\text{pH}$ assuming equilibrium at the standard hydrogen electrode, where $\mu_{\text{H}_2} = E_{\text{H}_2}^{\text{tot}} + \Delta\mu_{\text{H}_2}(T, 1 \text{ bar})$. Therefore, the

electrochemical potentials of O and OH can be readily calculated using the above electrochemical reactions as $\mu_{\text{OH}} = \mu_{\text{H}_2\text{O}} - (1/2\mu_{\text{H}_2} + eU_{\text{SHE}} - k_B T \ln(10)\text{pH})$ and $\mu_{\text{O}} = \mu_{\text{H}_2\text{O}} - (\mu_{\text{H}_2} + 2eU_{\text{SHE}} - 2k_B T \ln(10)\text{pH})$. Finally, it is common practice to replace the free energies of solid surfaces with or without adsorbates with total energies due to the small enthalpic and entropic contributions as compared to the gas-phase or liquid-phase molecules.³¹ Briefly, to validate this assumption, the vibrational entropy of adsorbed OH* and CO* atop are calculated to be 0.14 and 0.19 eV at 298 K, respectively. These values are not significant in comparison to the differences in binding energies as a function of the applied potential. Hence, the surface free energy of formation can be reformulated as

$$\Delta\gamma = \frac{1}{A_S}(\Delta E_{\text{ads}} - \sum_i n_i \Delta\mu_i(T, p, U)) \quad (9)$$

where ΔE_{ads} are the adsorption energies calculated using total energies. We set all temperatures $T = 298 \text{ K}$ in this study. Note that in this particular formulation the dependence of the free energy of adsorption on entropic contributions enters entirely through the corresponding dependence of the electrochemical potentials of the species in the reservoir on temperature, pressure, and electrode potential.

RESULTS AND DISCUSSION

Surface Phase Diagram of Au(111) Surface under Reaction Conditions. The surface phase diagram in Figure 1

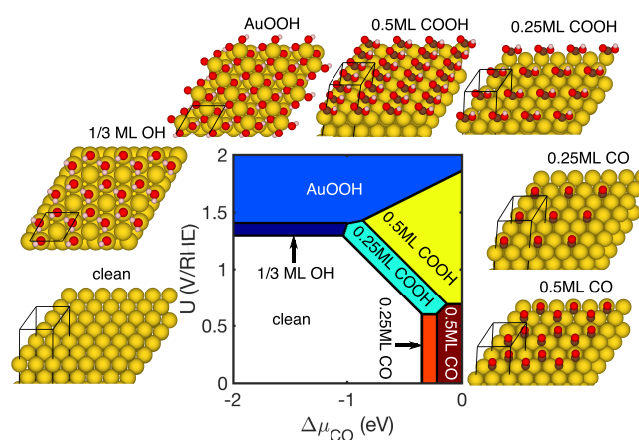


Figure 1. Surface phase diagram for the Au(111) surface as a function of applied potential and CO chemical potential. All binding energies are evaluated using neutral surfaces. For the atomic structures, Au is yellow, O is red, C is brown, and H is pink.

is constructed to investigate the surface state of Au(111) under the reaction conditions of CO electrooxidation. The surface free energy of formation per surface area for various surface phases was examined when constructing the surface phase diagram. The different regions appearing on the diagram correspond to different stable surface phases at given values of $\Delta\mu_{\text{CO}}$ and U/RHE . The binding energies of adsorbed species are calculated with neutral systems.

The clean Au(111) surface is found to be stable when the applied potential is lower than 1.3 V/RHE. Above 1.3 V, chemisorbed OH* becomes thermodynamically favorable on the Au(111) surface with a coverage of 1/3 of a monolayer (ML). In the model, the OH* is coadsorbed with water

molecules on a $\sqrt{3} \times \sqrt{3}$ supercell to form a honeycomb network of stabilizing hydrogen bonding.^{33,34} With a further increase of the applied potential to 1.4 V, the surface Au hydroxide (AuOOH) becomes stable. The structure of this AuOOH phase has also been reported previously.³⁴ A CO adsorption phase with 0.25 ML CO* and 0.5 ML CO* become thermodynamically stable when $\Delta\mu_{\text{CO}}$ is higher than -0.35 and -0.2 eV, respectively. The large area of clean Au(111) in the phase diagram indicates the noble nature of Au; water oxidation to OH* and CO adsorption only occurs with high positive potentials and high chemical potentials of CO. Interestingly, however, CO–OH bond formation is strongly promoted on the Au(111) surface. This can be seen in Figure 1 in that the COOH* surface phases occur at lower applied potentials and CO chemical potentials than the OH* and CO*-only phases. This observation is consistent with previous findings showing barrierless COOH formation on Au(111), which was attributed to the Au-mediated charge transfer from CO to OH.^{9,35} Because of the coadsorption between OH and CO, the adsorbed CO can be transformed to COOH at 0.6 V, which is significantly lower than the 1.3 V required for water oxidation to form OH*. The predicted 0.6 V is close to the onset potential of CO electrooxidation on Au(111) in acidic media. It is, however, still much higher than the onset potential of 0.2 V in alkaline media.¹¹ As stated earlier, the difference in onset potential in acidic versus alkaline media is attributed to the difference in the electric potential on the SHE scale at the same potential on the RHE scale. To bridge the gap between theory and experiment, we performed calculations to probe the potential-dependent binding energies of CO*, OH*, and COOH* using the double-reference method.

Potential-Dependent Adsorption Energies of Intermediates of CO Electrooxidation. The calculated total energies of bare Au(111) and the CO-adsorbed Au(111) slab at three different binding sites (fcc, bridge, and atop sites) as a function of U/SHE are shown in Figure 2a. The fitted parameters for the quadratic form of the potential-dependent total energies are included in Table 1. First, it can be seen that the PZC of Au(111) is predicted to be 0.46 V, which is consistent with the experimental value 0.53 V as measured in 0.1 M HClO₄.³⁶ The PZC calculated on the ($\sqrt{3} \times \sqrt{3}$)R30° Au(111) slab is 0.56 V; this difference could be due to the different *k*-point meshes used for different supercells. The reasonable PZC of Au(111) calculated with an implicit solvation model could be due to the fact that water layers above Au(111) are amorphous at PZC conditions, so there is little work function shift due to the orientation of the water layers.^{37,38} In contrast, water molecules adsorbed on the Pt(111) surface have been found to be important for evaluating the PZC accurately.^{38,39} The reason is that adsorbed water molecules induce a charge redistribution and form a surface dipole moment, shifting down the PZC. By use of DFT-based molecular dynamics, it has been observed that there are clear adsorption peaks at 2.5 Å above the surface in the water density profile on the Pt(111) surface, whereas these peaks are not present on the Au(111) surface.³⁸ Correspondingly, the charge redistribution induced by water adsorption is minimal on Au(111) surface.

With CO adsorption on Au(111), the work function and thus the PZC are shifted because of the induced surface dipole. Interestingly, the PZC shift depends upon the CO binding

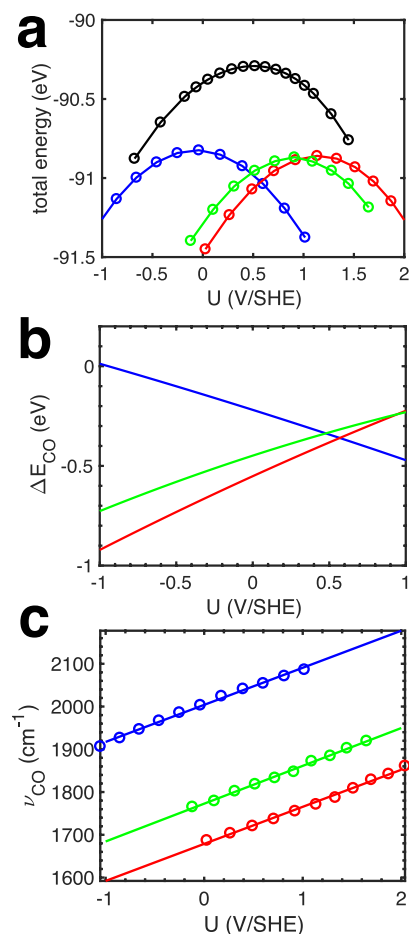


Figure 2. (a) Total energies of the bare Au(111) slab (black), CO adsorbed at an fcc site (CO-fcc: red), CO adsorbed at a bridge site (CO-bri: green), and CO adsorbed at an atop site (CO-atop: blue). The calculated total energies (circles) and polynomial fits (solid lines) are shown. (b) Adsorption energies of CO-fcc, CO-bri, and CO-atop. The CO adsorption energy is calculated as $\Delta E_{\text{CO}} = E_{\text{CO/slab}} - E_{\text{slab}} - E_{\text{CO}}$. (c) Vibration frequencies of C–O bond stretching of CO-fcc, CO-bri, and CO-atop.

Table 1. Fitted Parameters of the Quadratic Equation for Calculating the Total Energies of Various Models

model	U_0 (V)	C (e/V)	E_0 (eV)
$p(2 \times 2)$ Au (111) slab	0.46	0.92	−60.85
($\sqrt{3} \times \sqrt{3}$)R30° Au (111) slab	0.56	0.65	−45.86
1/3 ML OH	1.07	0.80	−95.64
AuOOH	0.76	0.87	−107.56
0.25 ML CO atop	−0.06	0.96	−90.82
0.25 ML CO fcc	1.12	1.00	−90.86
0.25 ML CO bri	0.89	1.04	−90.88
0.5 ML CO atop	0.21	1.02	−120.50
0.5 ML CO bri	1.08	1.00	−120.33
0.5 ML CO hcp fcc	1.29	0.96	−120.44
0.75 ML CO hcp fcc atop	1.00	0.86	−150.06
0.25 ML COOH atop	0.20	1.08	−112.93
0.5 ML COOH atop	−0.11	1.02	−163.87

sites. For the fcc and bridge sites, the PZC increases. For CO adsorbed on atop sites, the opposite trend is observed. The direction of the PZC shift can be directly attributed to the difference in the surface dipoles caused by CO adsorption. The

surface charge redistribution for CO adsorption on atop and fcc sites is shown in Figure 3; clearly adsorption at different

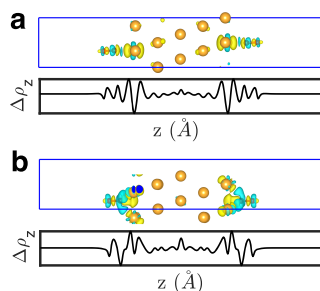


Figure 3. Isosurface plots of charge redistribution and x,y -plane integrated charge redistribution upon CO adsorption on the Au(111) surface at the (a) atop and (b) fcc sites. In the isosurface plot, cyan indicates negative charge and yellow indicates positive charge.

sites induces significantly different surface charge redistribution. By integrating the charge redistribution along the z -axis, we calculate surface dipoles of 0.44 and -0.19 D for the atop and fcc sites, respectively, consistent with the observed direction of the PZC shifts for these two CO binding sites. Atop CO is seen to induce electron transfer to Au, whereas fcc CO acquires electrons from Au, as can be seen by the different locations of the significant negative peaks in Figure 3.

As a result of the different sign of the PZC shifts, the binding energies of CO at different sites also change in different directions with respect to the applied electrode potential. In Figure 2b, we show that the binding energy of atop CO decreases with increasing electrode potential. On the other hand, the binding energies of CO at the fcc and bri sites increase with increasing potential. Consequently, atop CO becomes the most stable above 0.55 V, while fcc CO is the

most stable below 0.55 V. Another result of the potential-dependent CO binding energy is that the CO binding strength increases with pH. Specifically, at the same applied potential (0 V/RHE), the CO binding energies are -0.6 and -1.0 eV at pH = 0 and pH = 14, respectively. This theoretical prediction is consistent with the observed irreversible CO adsorption on Au(111) in base solution.¹⁴ We also calculated the vibrational frequency of the C=O bonding as a function of the electrode potential (Stark effect) as shown in Figure 2c. The vibrational frequencies of all adsorbed CO (in any binding site) increase as the electrode potential increases. This trend is consistent with experimental spectroscopic studies.¹⁴

Besides CO, two other important intermediates for CO electrooxidation are OH and COOH. We calculated adsorption energies of OH and COOH with respect to the applied potential as shown in Figure 4. The adsorption energy of OH increases with increasing potential, whereas the COOH adsorption energy decreases. However, compared to the change of CO adsorption energy with potential, the adsorption energy shifts for OH and COOH are less pronounced. The fitted parameters for calculated total energies for various adsorption phases are in Table 1.

Effects of pH on the Surface Phase Diagram of Au(111) Surface. We rebuild the surface phase diagram for different pH values by taking into account the potential-dependent adsorption energies for various adsorbates. The surface phase diagram at pH = 1 and pH = 13 are shown in Figure 5. The region of various surface states changes with pH values because the relative stabilities of different surface states changes. At pH = 1, it can be seen that the equilibrium potential for converting CO to COOH is 0.45 V/SHE, which is lower than 0.55 V/SHE at pH = 13. This result is inconsistent with the experimental observation that the onset potential in base is significantly lower than that in acid. Hence, the decrease of onset potential cannot be explained by the

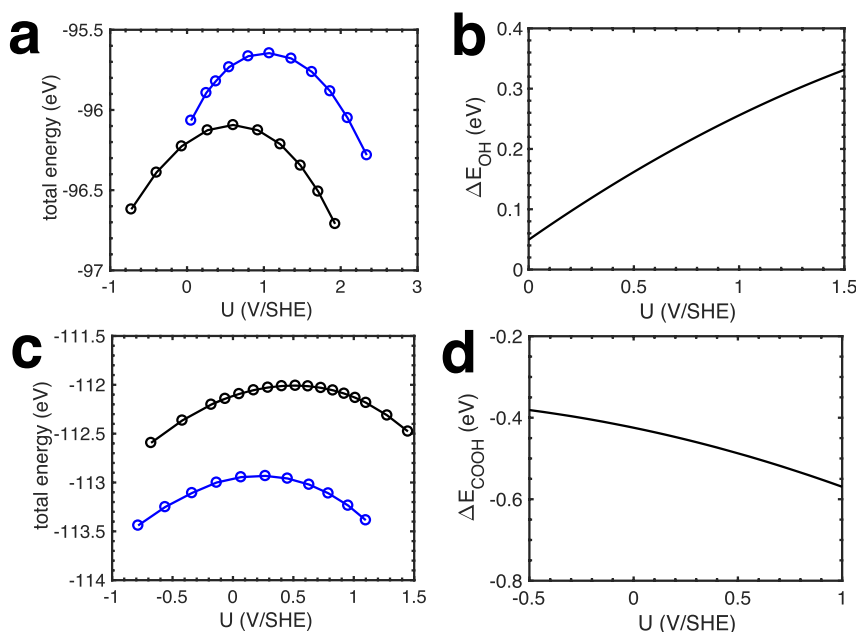


Figure 4. (a) Total energies of the clean Au(111) slab and with adsorbed OH*. (b) Binding energy of OH* as a function of applied potential. (c) Total energies of clean Au(111) slab and adsorbed COOH*. (d) Binding energy of COOH* as a function of applied potential. The binding energy of OH* is calculated as $\Delta E_{\text{OH}^*} = E_{\text{OH}^*/\text{slab}} - E_{\text{slab}} - E_{\text{H}_2\text{O}} + 0.5E_{\text{H}_2}$, and the binding energy of COOH* is calculated as $\Delta E_{\text{COOH}^*} = E_{\text{COOH}^*/\text{slab}} - E_{\text{slab}} - E_{\text{CO}} - E_{\text{H}_2\text{O}} + 0.5E_{\text{H}_2}$.

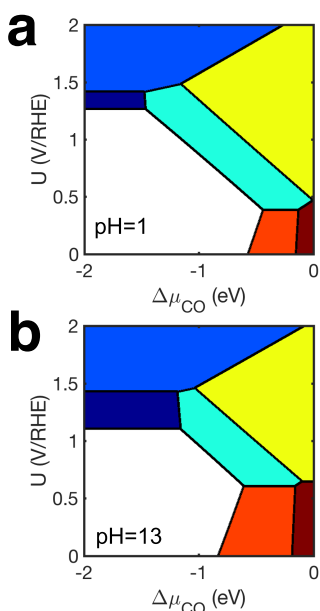
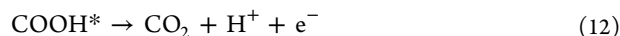
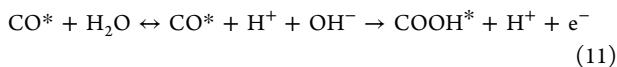


Figure 5. Surface phase diagram of Au(111) at pH = 1 and pH = 13. The stable phases are shown in Figure 1.

equilibrium potential decrease. In the next section, we employ microkinetic modeling to simulate the current density of CO electrooxidation as a function of the applied potential. We will see that the onset potential in base is dominated by other factors.

Microkinetic Modeling and the Reaction Mechanism of CO Electrooxidation on the Au(111) Surface. The reaction mechanism of CO electrooxidation is proposed as follows:



In the first step, CO is adsorbed on the Au surface. Then, CO* directly reacts with OH⁻ in solution, promoted by their attractive interaction, to form COOH. The adsorbed COOH* rapidly dehydrogenates to form CO₂. We calculated the current density associated with the COOH* formation step to represent the reactivity of the CO electrooxidation reaction since it is considered the rate-determining step. The current density is expressed as

$$\begin{aligned} j_{\text{COOH}^*} &= 2 \frac{F}{N_{\text{Au}}} N_{\text{Au}} \theta_{\text{CO}^*} \max([\text{OH}^-], \theta_{\text{OH}^*}) k_{\text{COOH}^*} \\ &= 2 \frac{F}{N_{\text{Au}}} N_{\text{Au}} \theta_{\text{CO}^*} \max([\text{OH}^-], \theta_{\text{OH}^*}) \frac{k_{\text{B}} T}{h} \exp(-\Delta G_{\text{COOH}^*}/k_{\text{B}} T) \end{aligned} \quad (13)$$

In eq 13, F is the Faraday constant, N_{A} is the Avogadro constant, N_{Au} is the number of Au site per cm², k_{B} is Boltzmann's constant, h is Planck's constant, θ_{CO^*} is the surface coverage of CO, $[\text{OH}^-]$ is the concentration of OH⁻ in solution, k_{COOH^*} is the rate constant of the COOH* formation step, and the temperature T is set to 298 K. Equation 13 is essentially the same as the Butler–Volmer equation which is normally employed for electrochemical kinetics where $\Delta G = z(E - E_0)$, where z is the number of electrons transferred and E_0 is the equilibrium potential for the reaction. θ_{CO^*} is calculated as $K_{\text{CO}^*} p_{\text{CO}} / (1 + K_{\text{CO}^*} p_{\text{CO}} + K_{\text{OH}^*})$ using the Langmuir adsorption model, in which K_{CO^*} is the equilibrium constant of CO adsorption, K_{OH^*} is the equilibrium constant of OH adsorption, and p_{CO} is the partial pressure of CO gas, which is set to 0.01 atm. Similarly, θ_{OH^*} is calculated as $K_{\text{OH}^*} / (1 + K_{\text{CO}^*} p_{\text{CO}} + K_{\text{OH}^*})$. $[\text{OH}^-]$ is equal to $10^{(\text{pH}-14)}$ M. k_{COOH^*} is calculated as $\frac{k_{\text{B}} T}{h} \exp(-\Delta G_{\text{COOH}^*}/k_{\text{B}} T)$, where ΔG_{COOH^*} is the reaction free energy of the COOH* formation step. Following the result that CO promotes its own oxidation,^{9,10} we propose that the adsorbed CO* can spontaneously bond

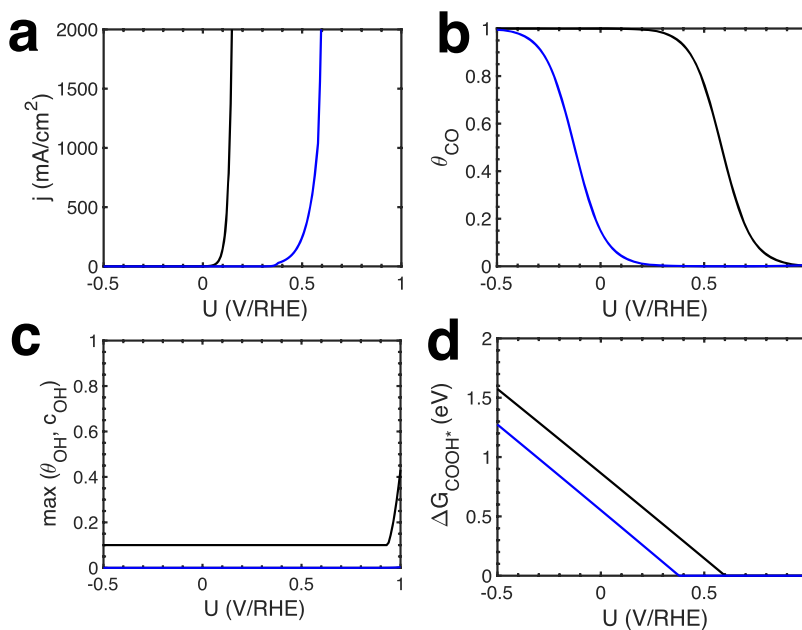


Figure 6. (a) Current density of CO electrooxidation reaction as a function of applied potential at pH = 1 (blue) and pH = 13 (black); (b) θ_{CO^*} ; (c) $\max([\text{OH}^-], \theta_{\text{OH}^*})$; and (d) ΔG_{COOH^*} , all calculated from our microkinetic model.

with nearby OH^- and OH^* to form COOH^* . In an alkaline solution, OH^- could be the oxidant due to its abundance in solution. In an acid solution, OH^* from water activation is more likely to be the oxidant. In our kinetic model, we assume an oxidant of OH^- in solution or OH^* on the surface, whichever is more abundant. Our proposed mechanism is similar to what is found from experiment.⁴⁰ In calculating the rate constant, ΔG_{COOH^*} is used instead of the energy barrier because CO^* and OH^-/OH^* bonding is barrierless.^{9,10} When ΔG_{COOH^*} is downhill, we set it to zero in our kinetic model.

The calculated current density from our microkinetic model is shown in Figure 6a. The onset potential for CO electrooxidation at pH = 13 is 0.1 V/RHE, whereas it is 0.5 V/RHE at pH = 1. The result is consistent with experimental observations.¹¹ The early onset potential in alkaline solution is due to a high concentration of reactants. First, the CO coverage is much higher at pH = 13 than that at pH = 1, as shown in Figure 6b. Specifically, at 0.1 V/RHE, θ_{CO^*} is 1 ML at pH = 13, whereas it is only 0.05 ML at pH = 1. Second, $[\text{OH}^-]$ is 12 orders of magnitude higher at pH 13 than at pH = 1 (see Figure 6c). We would like to emphasize that OH^- can directly participate in the reaction only because CO^* attracts OH^- from the solution to form COOH^* . As a result, OH^- does not require first adsorption on the electrode surface (on its own) to form OH^* . We can see from Figure 6d that ΔG_{COOH^*} is higher at pH = 13, so the reaction is not thermodynamically favorable in alkaline solution—the low onset potential in base is due to a high concentration of reactants. We also notice that the reaction mechanism of the CO electrooxidation reaction is different in acid versus base. In base, adsorbed CO directly reacts with $[\text{OH}^-]$ in solution due to the barrierless C–O bond formation on Au and its high concentration;⁴⁰ this is therefore an uncoupled electrochemical step. In acid, when a current is observed, the adsorbed CO reacts with adsorbed OH because θ_{OH^*} is higher than $[\text{OH}^-]$ at the onset potential. In this mechanism, OH^- must first be neutralized on Au to form OH^* at higher applied potentials, allowing for COOH^* formation through a chemical step on the surface.

To further support the above arguments, we have deliberately weakened the adsorption energy of CO at pH = 13 by 0.4 eV and show that the ΔG_{COOH^*} remains intact. The obtained current density as shown in Figure 7 has an onset potential higher than that of the original current density. This shift is clearly due to a decrease of θ_{CO^*} , which drops from 1

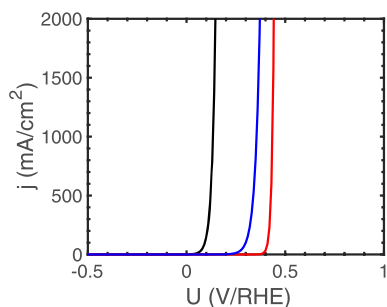


Figure 7. Sensitivity check of the dependence of the current density on θ_{CO^*} and $[\text{OH}^-]$. The black curve is the original current density at pH = 13. The blue curve is obtained by weakening the CO adsorption energy by 0.4 eV. The red curve is obtained by using θ_{OH^*} instead of $[\text{OH}^-]$.

ML to 2×10^{-4} ML at 0.1 V/RHE. On the other hand, if we assume the adsorbed OH^* is the reactant rather than the OH^- in solution, by replacing $[\text{OH}^-]$ with θ_{OH^*} in the microkinetic model at pH = 13, then at 0.1 V/RHE, θ_{OH^*} is as low as 4×10^{-15} ML, leading to a significant increase in the onset potential as shown in Figure 7. This analysis shows that the high concentration of OH^- is essential for CO oxidation activity at low applied potentials.

CONCLUSION

In the study, we employed DFT calculations and the double-reference method to simulate the Au(111)/aqueous interface under the reaction conditions of CO electrooxidation. We calculated the potential-dependent adsorption energies of the intermediates and reaction energies of the elementary steps and were able to explain the observed lower onset potential for CO electrooxidation on Au(111) in alkaline solution than in acid solution. We show that there are three significant reasons for the low onset potential in alkaline conditions. First, CO adsorption on Au(111) is stronger in base as compared to an acid solution for the same applied potential in the RHE scale, which leads to a higher CO coverage on Au(111) in the alkaline solution. Second, CO attracts OH^- in the electrolyte to form COOH^* . Finally, the concentration of OH^- is high in alkaline electrolyte, increasing the interaction rate with adsorbed CO to form COOH^* . The lower onset potential for CO electrooxidation in alkaline media was confirmed by microkinetic modeling using the DFT calculated reaction energetics.

ASSOCIATED CONTENT

Supporting Information

The Supporting Information is available free of charge on the ACS Publications website at DOI: 10.1021/acs.langmuir.8b03644.

Figures S1–S3 (PDF)

AUTHOR INFORMATION

Corresponding Author

*E-mail: henkelman@utexas.edu.

ORCID

Graeme Henkelman: 0000-0002-0336-7153

Notes

The authors declare no competing financial interest.

ACKNOWLEDGMENTS

This work is supported by the Department of Energy under Contract DE-SC0010576 and the Welch Foundation under Grant F-1841. The calculations were done at the National Energy Research Scientific Computing Center and the Texas Advanced Computing Center.

REFERENCES

- (1) Sheng, W.; Zhuang, Z.; Gao, M.; Zheng, J.; Chen, J. G.; Yan, Y. Correlating hydrogen oxidation and evolution activity on platinum at different pH with measured hydrogen binding energy. *Nat. Commun.* **2015**, *6*, 5848.
- (2) Hori, Y.; Takahashi, R.; Yoshinami, Y.; Murata, A. Electrochemical Reduction of CO at a Copper Electrode. *J. Phys. Chem. B* **1997**, *101*, 7075–7081.
- (3) Kuhl, K. P.; Hatsukade, T.; Cave, E. R.; Abram, D. N.; Kibsgaard, J.; Jaramillo, T. F. Electrocatalytic Conversion of Carbon

Dioxide to Methane and Methanol on Transition Metal Surfaces. *J. Am. Chem. Soc.* **2014**, *136*, 14107–14113.

(4) Schouten, K. J. P.; Pérez Gallent, E.; Koper, M. T. The influence of pH on the reduction of CO and CO₂ to hydrocarbons on copper electrodes. *J. Electroanal. Chem.* **2014**, *716*, 53–57.

(5) Xiao, H.; Cheng, T.; Goddard, W. A.; Sundaraman, R. Mechanistic Explanation of the pH Dependence and Onset Potentials for Hydrocarbon Products from Electrochemical Reduction of CO on Cu (111). *J. Am. Chem. Soc.* **2016**, *138*, 483–486.

(6) Cheng, T.; Wang, L.; Merinov, B. V.; Goddard, W. A. Explanation of Dramatic pH-Dependence of Hydrogen Binding on Noble Metal Electrode: Greatly Weakened Water Adsorption at High pH. *J. Am. Chem. Soc.* **2018**, *140*, 7787–7790.

(7) Hussain, J.; Jónsson, H.; Skúlason, E. Calculations of Product Selectivity in Electrochemical CO₂ Reduction. *ACS Catal.* **2018**, *8*, 5240–5249.

(8) Zhao, M.; Anderson, A. B. Predicting pH dependencies of electrode surface reactions in electrocatalysis. *Electrochem. Commun.* **2016**, *69*, 64–67.

(9) Rodríguez, P.; Koverga, A. A.; Koper, M. T. M. Carbon Monoxide as a Promoter for its own Oxidation on a Gold Electrode. *Angew. Chem., Int. Ed.* **2010**, *49*, 1241–1243.

(10) Koverga, A. A.; Frank, S.; Koper, M. T. M. Density Functional Theory study of electric field effects on CO and OH adsorption and co-adsorption on gold surfaces. *Electrochim. Acta* **2013**, *101*, 244–253.

(11) Rodríguez, P.; Garcia-Araez, N.; Koper, M. T. M. Self-promotion mechanism for CO electrooxidation on gold. *Phys. Chem. Chem. Phys.* **2010**, *12*, 9373.

(12) Rodríguez, P.; Feliu, J. M.; Koper, M. T. M. Unusual adsorption state of carbon monoxide on single-crystalline gold electrodes in alkaline media. *Electrochem. Commun.* **2009**, *11*, 1105–1108.

(13) Rodríguez, P.; Kwon, Y.; Koper, M. T. M. The promoting effect of adsorbed carbon monoxide on the oxidation of alcohols on a gold catalyst. *Nat. Chem.* **2012**, *4*, 177–182.

(14) Rodríguez, P.; Garcia-Araez, N.; Koverga, A.; Frank, S.; Koper, M. T. M. CO electrooxidation on gold in alkaline media: A combined electrochemical, spectroscopic, and DFT study. *Langmuir* **2010**, *26*, 12425–12432.

(15) Kresse, G.; Hafner, J. Ab initio molecular dynamics for liquid metals. *Phys. Rev. B: Condens. Matter Mater. Phys.* **1993**, *47*, 558.

(16) Kresse, G.; Furthmüller, J. Efficiency of ab-initio total energy calculations for metals and semiconductors using a plane-wave basis set. *Comput. Mater. Sci.* **1996**, *6*, 15–50.

(17) Kresse, G.; Furthmüller, J. Efficient iterative schemes for ab initio total-energy calculations using a plane-wave basis set. *Phys. Rev. B: Condens. Matter Mater. Phys.* **1996**, *54*, 11169.

(18) Perdew, J. P.; Wang, Y. Accurate and simple analytic representation of the electron-gas correlation energy. *Phys. Rev. B: Condens. Matter Mater. Phys.* **1992**, *45*, 13244.

(19) Kresse, G.; Joubert, D. From ultrasoft pseudopotentials to the projector augmented-wave method. *Phys. Rev. B: Condens. Matter Mater. Phys.* **1999**, *59*, 1758–1775.

(20) Monkhorst, H. J.; Pack, J. D. Special points for Brillouin-zone integrations. *Phys. Rev. B* **1976**, *13*, 5188–5192.

(21) Taylor, C. D.; Wasileski, S. A.; Filhol, J.-S.; Neurock, M. First principles reaction modeling of the electrochemical interface: Consideration and calculation of a tunable surface potential from atomic and electronic structure. *Phys. Rev. B: Condens. Matter Mater. Phys.* **2006**, *73*, 165402.

(22) Filhol, J.-S.; Neurock, M. Elucidation of the Electrochemical Activation of Water over Pd by First Principles. *Angew. Chem., Int. Ed.* **2006**, *45*, 402–406.

(23) Fishman, M.; Zhuang, H. L.; Mathew, K.; Dirschka, W.; Hennig, R. G. Accuracy of exchange-correlation functionals and effect of solvation on the surface energy of copper. *Phys. Rev. B: Condens. Matter Mater. Phys.* **2013**, *87*, 245402.

(24) Mathew, K.; Sundaraman, R.; Letchworth-Weaver, K.; Arias, T. A.; Hennig, R. G. Implicit solvation model for density-functional

study of nanocrystal surfaces and reaction pathways. *J. Chem. Phys.* **2014**, *140*, 084106.

(25) Steinmann, S. N.; Sautet, P. Assessing a First-Principles Model of an Electrochemical Interface by Comparison with Experiment. *J. Phys. Chem. C* **2016**, *120*, 5619–5623.

(26) Steinmann, S. N.; Michel, C.; Schwiedernoch, R.; Sautet, P. Impacts of electrode potentials and solvents on the electroreduction of CO₂: a comparison of theoretical approaches. *Phys. Chem. Chem. Phys.* **2015**, *17*, 13949–13963.

(27) Trasatti, S. Structure of the metal/electrolyte solution interface: new data for theory. *Electrochim. Acta* **1991**, *36*, 1659–1667.

(28) Mamatkulov, M.; Filhol, J.-S. An abinitio study of electrochemical vs. electromechanical properties: the case of CO adsorbed on a Pt(111) surface. *Phys. Chem. Chem. Phys.* **2011**, *13*, 7675–7684.

(29) Nørskov, J. K.; Rossmeisl, J.; Logadottir, A.; Lindqvist, L.; Kitchin, J. R.; Bligaard, T.; Jónsson, H. Origin of the overpotential for oxygen reduction at a fuel-cell cathode. *J. Phys. Chem. B* **2004**, *108*, 17886–17892.

(30) Hansen, H. A.; Rossmeisl, J.; Nørskov, J. K. Surface Pourbaix diagrams and oxygen reduction activity of Pt, Ag and Ni(111) surfaces studied by DFT. *Phys. Chem. Chem. Phys.* **2008**, *10*, 3722.

(31) Reuter, K.; Scheffler, M. Composition and structure of the RuO₂ surface in an O₂ and CO environment: Implications for the catalytic formation of CO₂. *Phys. Rev. B: Condens. Matter Mater. Phys.* **2003**, *68*, 045407.

(32) Chase, M. W. J. *NIST-JANAF Thermochemical Tables*, 4th ed.; American Institute of Physics: New York, 1998.

(33) Lew, W.; Crowe, M. C.; Campbell, C. T.; Carrasco, J.; Michaelides, A. The Energy of Hydroxyl Coadsorbed with Water on Pt(111). *J. Phys. Chem. C* **2011**, *115*, 23008–23012.

(34) Diaz-Morales, O.; Calle-Vallejo, F.; de Munck, C.; Koper, M. T. M. Electrochemical water splitting by gold: evidence for an oxide decomposition mechanism. *Chem. Sci.* **2013**, *4*, 2334–2343.

(35) Koverga, A. A.; Frank, S.; Koper, M. T. M. Density Functional Theory study of electric field effects on CO and OH adsorption and co-adsorption on gold surfaces. *Electrochim. Acta* **2013**, *101*, 244–253.

(36) Hamm, U.; Kramer, D.; Zhai, R.; Kolb, D. The pzc of Au(111) and Pt(111) in a perchloric acid solution: an ex situ approach to the immersion technique. *J. Electroanal. Chem.* **1996**, *414*, 85–89.

(37) Schnur, S.; Groß, A. Properties of metal-water interfaces studied from first principles. *New J. Phys.* **2009**, *11*, 125003.

(38) Le, J.; Iannuzzi, M.; Cuesta, A.; Cheng, J. Determining Potentials of Zero Charge of Metal Electrodes versus the Standard Hydrogen Electrode from Density-Functional-Theory-Based Molecular Dynamics. *Phys. Rev. Lett.* **2017**, *119*, 016801.

(39) Jinnouchi, R.; Anderson, A. B. Electronic structure calculations of liquid-solid interfaces: Combination of density functional theory and modified Poisson-Boltzmann theory. *Phys. Rev. B: Condens. Matter Mater. Phys.* **2008**, *77*, 245417.

(40) Rodríguez, P.; Garcia-Araez, N.; Koper, M. T. M. Self-promotion mechanism for CO electrooxidation on gold. *Phys. Chem. Chem. Phys.* **2010**, *12*, 9373–9380.